BRITISH JOURNAL OF HOSPITAL MEDICINE

REVIEW

Ring-Enhancing Lesions—Differentiation with MRI

Elif Peker[1,*], Sena Ünal[1], Sena Bozer Uludağ[1], Nil Sezer Yılmazer Zorlu[1]

[1]Department of Radiology, Ankara University Medical School, Ankara, Turkey
*Correspondence: elifozyurek0@yahoo.com (Elif Peker)

Abstract

Lesions with central hypointensity and peripheral contrast enhancement are defined as ring-enhancing lesions. The aetiologies of ring-enhancing lesions may be various, including infections, tumours, demyelinating diseases, treatment-related conditions and hematoma. The imaging findings and their distinguishing features also vary among different ring-enhancing lesions. This review examines the magnetic resonance imaging findings of different ring-enhancing lesions and their distinguishing features.

Key words: magnetic resonance imaging (MRI); ring-enhancing; glioblastoma; metastasis; radiation necrosis; infection

Submitted: 20 April 2024 Revised: 25 July 2024 Accepted: 5 August 2024

Introduction

A brain lesion with an open ring or irregular or smooth contrast enhancement at the periphery and a lack of contrast enhancement in the central part, with hypodensity/hypointensity on computed tomography (CT) and magnetic resonance imaging (MRI), is called a ring-enhancing lesion (Chan and Siu, 2021). Ring-enhancing lesions constitute a large part of a neuroradiologist's daily practice. The nonspecific clinical symptoms of these lesions make clinical diagnosis difficult. Delay in treatment in this disease group, which includes tumours, demyelinating lesions and infections, can lead to neurological sequelae and even death. Making a radiological diagnosis is especially important in this disease group, as clinical diagnosis is challenging. Here, we provide an overview of the classical imaging patterns of infections, tumours, treatment-related changes and ischemic and demyelinating pathologies which may cause ring enhancement. We survey the diagnostic performances of MRI techniques, such as diffusion-weighted imaging (DWI) with apparent diffusion coefficient (ADC) maps, magnetic resonance spectroscopy (MRS) and perfusion MRI. In this review, our aim is to present the MRI findings of different ring-enhancing lesions and their distinguishing features.

Infectious Causes

While pyogenic abscesses and hydatid cysts are usually observed as single lesions, fungal abscesses, cerebral toxoplasmosis, neurocysticercosis and turberculomas are often multiple lesions (Chan and Siu, 2021; Luthra et al, 2007; Marcus et al, 2021; Padayachy and Ozek, 2023).

How to cite this article:
Peker E, Ünal S, Uludağ SB, Zorlu NSY. Ring-Enhancing Lesions—Differentiation with MRI. Br J Hosp Med. 2024. https://doi.org/10.12968/hmed.2024.0195

Localisation

Pyogenic abscesses, neurocysticercosis and toxoplasmosis tend to localise in the grey-white matter junctions (Fig. 1) (Luthra et al, 2007). Fungal abscess and cerebral toxoplasmosis may involve the basal ganglia; however, pyogenic abscesses rarely involve the basal ganglia (Chan and Siu, 2021; Luthra et al, 2007; Marcus et al, 2021) (Fig. 2). In neurocysticercosis, lesions may be located in the subarachnoid space and ventricles (Chan and Siu, 2021). Pyogenic abscesses are located especially in the anterior and middle cerebral artery vascular territories, while toxoplasma is located in the frontoparietal regions and thalamus (Luthra et al, 2007).

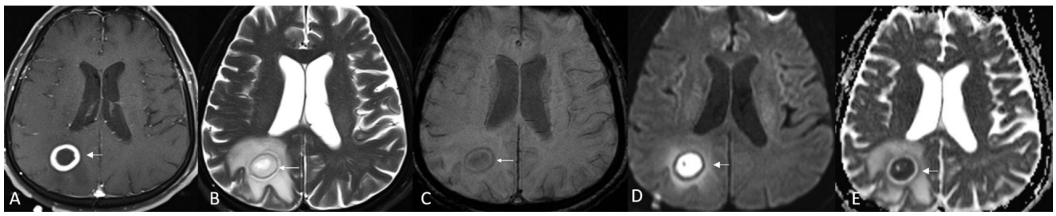

Fig. 1. A 71-year-old man with a right parietal pyogenic abscess at the grey-white matter junction. (A) Axial contrast-enhanced T1-weighted image shows a rim-enhancing mass in the right parietal lobe (arrow). (B) Axial T2-weighted image, a complete hypointense peripheral rim (arrow) is present. (C) On axial susceptibility-weighted imaging (SWI), the abscess is bordered by two concentric rims, with the outer one being hypointense (arrow) and the inner one hyperintense (arrowhead), forming the dual rim sign. (D) On axial diffusion-weighted imaging (DWI), the central core of the abscess is hyperintense and the peripheral rim is hypointense (arrow). (E) On the axial apparent diffusion coefficient (ADC) map, the peripheral rim is hyperintense and the central core of the abscess is hypointense, suggesting diffusion restriction (arrow).

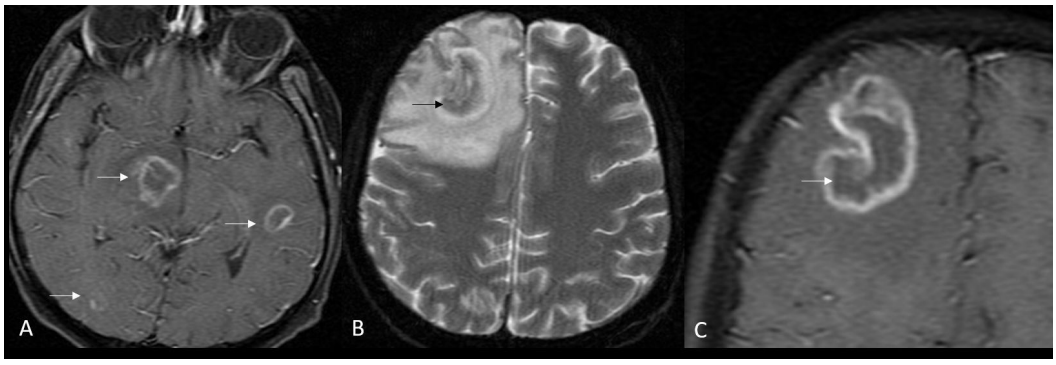

Fig. 2. A 19-year-old man with acute myeloid leukaemia. (A) Multiple peripheral enhancing fungal abscesses can be seen at the grey-white matter junctions and right thalamus (arrows). Involvement of deep grey matter suggests a fungal abscess over a pyogenic abscess. (B) The lesion is T2 hypointense in the central part (arrow). (C) The T2 hypointense central component is not enhancing (arrow).

Imaging Findings

While the outer edges of both pyogenic abscess and tuberculoma are smooth or lobulated (100% or 90%, respectively), jagged edges of a lesion suggest a fungal

abscess (Luthra et al, 2007). The centre of a pyogenic abscess is hyperintense on T2 weighted image (WI) (Fig. 1) (Luthra et al, 2007). In tuberculomas, the central lesion is often hypo/isointense, but if liquefied material is present, it can also be observed as hyperintense on T2WI (Luthra et al, 2007). The signal intensity on T2WI of the central part of cerebral toxoplasmosis lesions can vary (Chan and Siu, 2021). If present, a 'concentric sign', consisting of concentric hypointense and hyperintense zones on T2WI, suggests cerebral toxoplasmosis (Marcus et al, 2021). Fungal abscesses are distinguished from other abscesses by T2-hypointense, non-enhancing intracavitary extensions (Chan and Siu, 2021; Luthra et al, 2007) that extend from the wall to the centre. Due to these extensions, hypointense areas on T2WI are observed in the centre of the fungal abscess lesion, which is actually hyperintense on T2WI (Chan and Siu, 2021; Luthra et al, 2007). Fungal abscesses are not suppressed on fluid-attenuated inversion recovery (FLAIR) images (Chan and Siu, 2021).

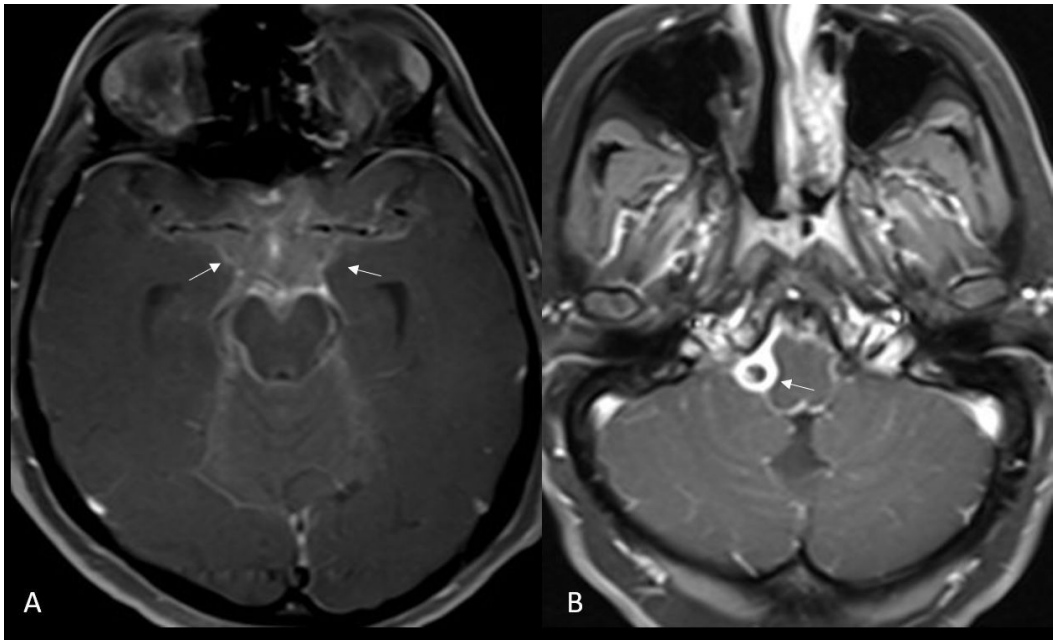

Fig. 3. A 42-year-old woman with hemiparesis, tuberculosis meningitis and tuberculoma. (A) Axial post-contrast image shows leptomeningeal enhancement around the basal cisterns, suggesting tuberculosis meningitis (arrows). (B) Follow-up axial post-contrast magnetic resonance imaging (MRI) shows a peripheral enhancing lesion at the right cerebellopontine cistern, suggesting tuberculoma (arrow). The presence of concomitant leptomeningeal enhancement at the basal cisterns suggests central nervous system tuberculosis. MRI, magnetic resonance imaging.

The centre of a hydatid cyst is hyperintense on T2WI, mostly uniloculated and sometimes multiloculated (Işık et al, 2024). The enhancing wall of a pyogenic abscess is thin and more prominent in the medial wall (Chan and Siu, 2021). The presence of daughter abscesses in the proximity of the medial wall is an important feature of pyogenic abscesses (Luthra et al, 2007). In a pyogenic abscess, the susceptibility-weighted imaging (SWI) sequence shows a dual rim sign consisting of a hypointense ring at the periphery of the lesion and a hyperintense ring inside

(Fig. 1) (Toh et al, 2012). In tuberculoma cases, in addition to ring-enhancing lesions, solid lesions can also be observed. Leptomeningeal contrast enhancement in the basal cisterns is a finding that can be evaluated in favour of a tuberculoma (Fig. 3).

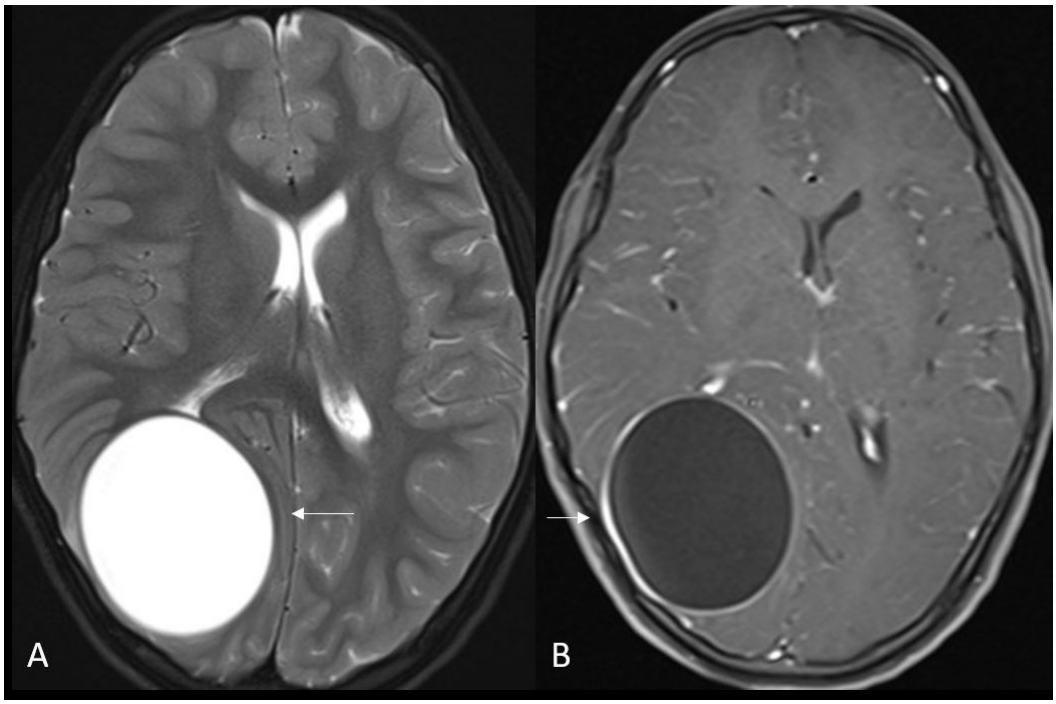

Fig. 4. An 18-year-old boy. (A) Axial T2-weighted image shows a well-defined T2 hyperintense uniloculated lesion, without perilesional oedema (arrow). (B) Axial post-contrast T1-weighted image shows linear enhancement at the periphery of the lesion (arrow).

The walls of neurocysticercosis lesions are thin (Chan and Siu, 2021). Although the appearance of neurocysticercosis varies depending on the stage of the lesion, it typically occurs in the form of calcific nodules, which are hypointense on T2WI, without surrounding oedema (Chan and Siu, 2021). In one-third of cerebral toxoplasmosis cases, an eccentric enhancing core is observed, giving the lesion the appearance of an eccentric mural nodule with central hypointensity and peripheral enhancement (Chan and Siu, 2021). Hydatid cysts are typically thin-walled (Fig. 4) (Padayachy and Ozek, 2023). Although the size of the lesion is large in hydatid cysts, oedema is either absent or minimal (Padayachy and Ozek, 2023). The most distinctive feature of a pyogenic abscess is the restriction in the centre of the lesion on DWI due to the accumulation of inflammatory cells and bacteria (Fig. 1) (Chan and Siu, 2021; Luthra et al, 2007). In a fungal abscess, diffusion restriction is observed in the lesion wall and its internal projections (Chan and Siu, 2021; Luthra et al, 2007). The diffusion restriction observed in fungal abscesses is more pronounced than in pyogenic abscesses (0.50 ± 0.05 vs $0.73 \pm 0.18 \times 10^{-3}$ mm^2/s, $p = 0.010$). Diffusion restriction is not frequently observed in hydatid cysts, tuberculomas or toxoplasmosis (Fig. 5) (Chan and Siu, 2021; Luthra et al, 2007). Low relative cerebral blood volume (rCBV) values compared to parenchyma have been

reported in cerebral toxoplasmosis and pyogenic abscesses (Chan and Siu, 2021). Tuberculomas can be distinguished from other infections by their peripheral hyperperfusion (Fig. 5) (Sankhe et al, 2013).

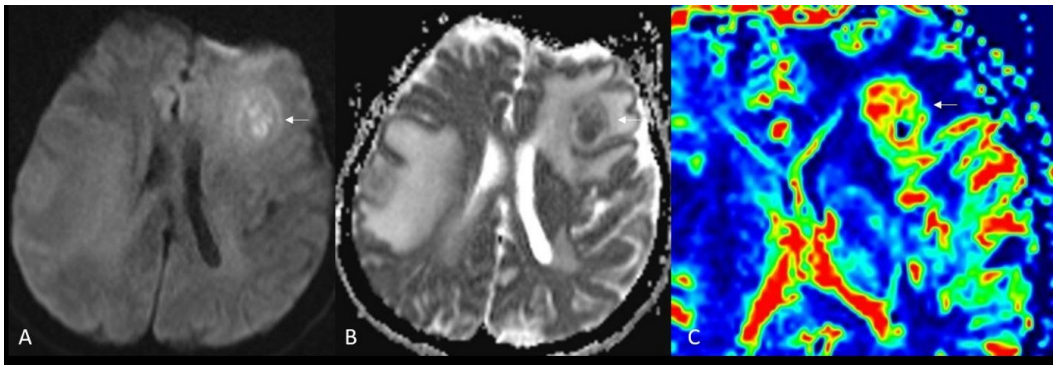

Fig. 5. A 65-year-old woman with tuberculoma. (A,B) Axial diffusion-weighted image and ADC map show diffusion restriction in the tuberculoma (arrows). (C) Perfusion image shows hyperperfusion (arrow).

Differential Diagnosis

While the hypointense ring is complete in abscesses, the ring is mostly incomplete in demyelinating pathologies (Toh et al, 2012). A dual rim finding is the most specific finding distinguishing pyogenic brain abscess from necrotic glioblastoma (GBM), as it is not detected in GBM (Toh et al, 2012). The patient's immunocompromise may be a clue for a fungal abscess, and human immunodeficiency virus (HIV) positivity may be a clue for toxoplasmosis (Chan and Siu, 2021) (Fig. 5). Cerebral toxoplasmosis, which is often confused with lymphoma, can be distinguished by perfusion MRI (Marcus et al, 2021). Lower rCBV values have been reported in cerebral toxoplasmosis (<1.5). In a perfusion MRI examination, the centre of the tuberculomas is hypoperfused and the periphery is hyperperfused (Fig. 6) (Sankhe et al, 2013). With this feature, a value of rCBV ≥ 3.745 can be used as a threshold to distinguish tuberculoma from metastasis (Sankhe et al, 2013).

Demyelinating Diseases

A tumefactive demyelinating lesion (TDL) is an atypical form of multiple sclerosis (MS) that mimics a high-grade glial tumour (French, 2021). Distinguishing between these two pathologies is important to prevent complications that may occur due to surgery (French, 2021). The sensitivity and specificity of MRI are 84% and 94%, respectively, for differentiating between a TDL and a tumour (Nakayama et al, 2021). Even if all the distinguishing features are examined, the most careful eyes may not be able to distinguish clearly between a tumour and an infection (Seewann et al, 2008). If another lesion is evident on the MRI that may suggest demyelinating pathology or/and if the lumbar punction (LP) findings are positive, the patient may be given short-term steroids and monitored for clinical improvement (French, 2021). However, it should be kept in mind that cerebrospinal fluid-specific oligo-

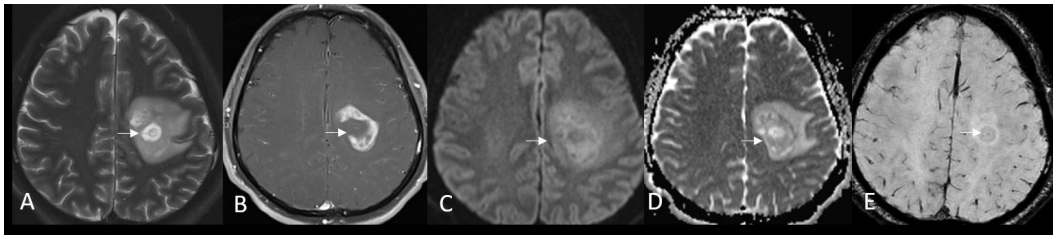

Fig. 6. A 23-year-old male with Balo's concentric sclerosis. (A) Axial T2 weighted image shows a round lesion with irregular, alternating bands of hyperintense and isointense signals, representing myelinating and demyelinating areas (arrow). The lesion is surrounded by oedema. (B) Axial contrast-enhanced MRI shows open ring enhancement, with the non-enhancing side on the cortical side and the enhanced side on the white matter side, secondary to the active demyelinating process, which is a very specific finding (arrow). (C,D) DWI and ADC maps show high ADC values in the centre of the lesion due to vasogenic oedema and myelin destruction, while low ADC values are detected in the periphery due to inflammatory cell infiltration (arrows). (E) SWI image shows a central vein sign, which is a specific biomarker of perivenous inflammatory demyelination (arrow).

clonal bands are positive in 30–80% of the cases, not in all (French, 2021). Patients who have no other supporting findings on MRI, whose LP is negative and whose clinical condition worsens should be evaluated for biopsy (French, 2021).

Imaging Findings

TDL is most commonly observed as a single, large ring-enhancing lesion located in the frontal and parietal lobes (41–74%), accompanied by oedema, and causing a mass effect (French, 2021; Nakayama et al, 2021). Observation of open ring enhancement, with the non-enhancing side on the cortical side and the enhanced side on the white-matter side, secondary to the active demyelinating process, is a very specific finding (specificity: 98–100%), but its sensitivity is lower (27–71%) (Chan and Siu, 2021; Kim et al, 2009). The incidence of incomplete ring enhancement is higher than the incidence of complete peripheral enhancement (35% vs 18%) (Altintas et al, 2012; Fereidan-Esfahani et al, 2022; Nakayama et al, 2021). The ring enhancement observed in infections and tumours is more irregular and thicker (Seewann et al, 2008). The presence of other lesions accompanying the larger lesion is suggestive of demyelinating pathology, while less or no mass effect and oedema (67% and 57%, respectively), a hypointense ring on T2WI (48%), a smaller size than tumours (27.4 ± 14.3 mm vs 42 ± 16.2 mm, $p < 0.001$) and high ADC values are other findings indicating a demyelinating pathology (French, 2021; Nakayama et al, 2021; Seewann et al, 2008).

In TDL, the hypointensity detected in T2WI and T2* images at the periphery of the lesion is less obvious than in tumours and infections (Seewann et al, 2008). In half of the cases, diffusion restriction is observed in any part of the lesion (Fereidan-Esfahani et al, 2022). High ADC values are detected in the centre of the lesion due to vasogenic oedema and myelin destruction, and low ADC values are detected in the periphery due to inflammatory cell infiltration (Malhotra et al, 2009; Nakayama et al, 2021). Unlike abscesses and tumours, in TDL, follow-up MRI examinations show diffusion restriction changes over time due to the active demyelination process at the edges of the lesion (Abou Zeid et al, 2012; Nakayama et al, 2021). The

presence of a centrally located venous structure in the form of dots or lines, smaller than 2 mm, in at least two planes on an SWI sequence or T2* images within the white matter lesion is called a central vein sign and is a specific biomarker of perivenous inflammatory demyelination (Nakayama et al, 2021). A central vein sign is seen in 80–92% of all MS lesions (Nakayama et al, 2021).

Atypical Idiopathic Inflammatory Demyelinating Lesions

According to their morphological findings on MRI, atypical idiopathic inflammatory demyelinating lesions (IIDLs) can be divided into 4 groups: megacystic, Balo-like, infiltrative and ring-like (Wallner-Blazek et al, 2013). The megacystic type is a cyst-like single lesion, larger than 3 cm, located in the hemispheric white matter and extending along the cortical ribbon (Wallner-Blazek et al, 2013). Infiltration of the adjacent cortex and lack of thickening in the cortex are findings that exclude a tumour (Seewann et al, 2008). The infiltrative type usually consists of a single lesion that is large, poorly circumscribed, heterogeneously enhancing, and suggestive of a diffuse infiltrative process (Wallner-Blazek et al, 2013). These lesions may grow slowly within 2–6 weeks, and their contrast enhancement may vary. High doses of steroids have little effect on these lesions (Seewann et al, 2008). Balo-like IIDLs are usually multiple lesions consisting of multiple concentric rings and two or more bands of different signal intensities in any sequence (Seewann et al, 2008) (Fig. 6). They show little or no mass effect (Wallner-Blazek et al, 2013). A ring-like lesion consists of single or multiple ring-enhanced lesions, with a hypointense ring that is more subtle than the abscess observed on T2WI and T2* images (Seewann et al, 2008). The lesions are accompanied by oedema, but the mass effect is either absent or minimal (Wallner-Blazek et al, 2013). In megacystic and infiltrating types, excluding the tumoral and infectious process may not always be possible (Wallner-Blazek et al, 2013). Peripheral contrast enhancement is not as irregular and thick as expected in tumours (Seewann et al, 2008). Specific features, such as the absence of lumbar puncture findings, the absence of other accompanying MS lesions and the fact that the lesion continues to grow despite high-dose steroid treatment, do not definitely rule out TDL (Seewann et al, 2008). A formula has been proposed to distinguish TDL and high-grade glioma: (gender $\times$ 2) – (age $\times$ 0.05) + (presentation $>$7 weeks $\times$ 2) + (none or mild oedema $\times$ 5) + (T2 hypointense rim $\times$ 2) – 4 = x (female: 1, presentation $>$7 weeks: 1, none or mild oedema: 1, presence of T2 hypointense rim: 1) (French, 2021). If x is a positive number, the probability of TDL is higher; otherwise, it is a tumoral lesion (French, 2021) (Figs. 7,8).

Tumoral Causes

The three most common tumour types with ring enhancement in the brain are GBM, primary central nervous system lymphoma (PCNSL) and metastasis. Metastasis is the most common brain tumour in adults. The presence of multiple lesions is more common in GBM than in lymphoma or metastasis (85.2% vs 44.4%) (Hung et al, 2023; Meier et al, 2020).

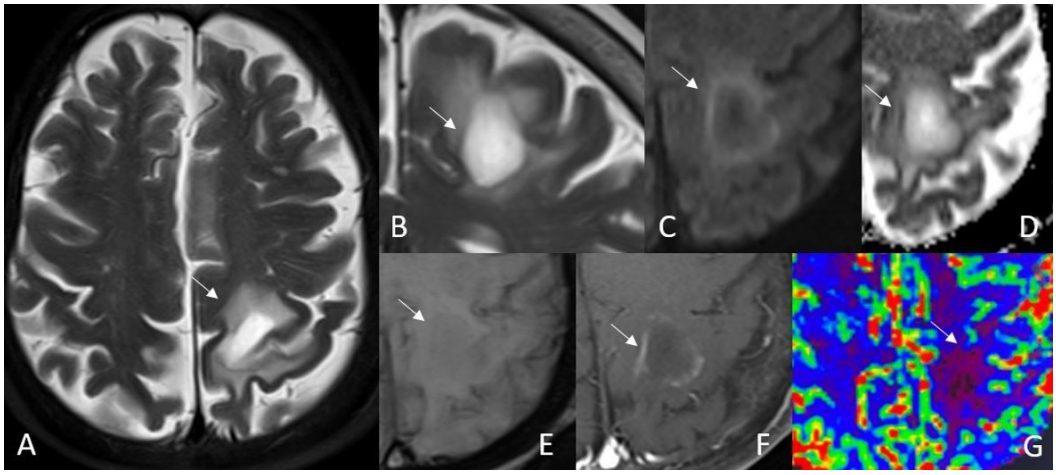

Fig. 7. A 61-year-old female patient with a tumefactive demyelinating lesion complaining of right hemiparesis that had been progressing for 3 weeks underwent MRI with a preliminary diagnosis of glial tumour. (A) The axial plane T2-weighted image shows a lesion located at the left frontoparietal lobes, involving the pre- and postcentral gyri, and accompanied by mild oedema (arrow). (B) Periphery of the lesion is T2 hypointense (arrow) on a T2 weighted coronal image. (C,D) DWI and ADC maps show diffusion restriction at the periphery (arrows). (E) No intratumoural susceptibility is observed in the lesion on the SWI (arrow). (F) The post-contrast image lesion shows open ring enhancement (arrow). (G) Lesion is hypoperfused on the perfusion image (arrow). Using the equation mentioned in the text, we found $(1 \times 2) - (61 \times 0.05) + 0 + (1 \times 5) + (1 \times 2) - 4 = 1.95$.

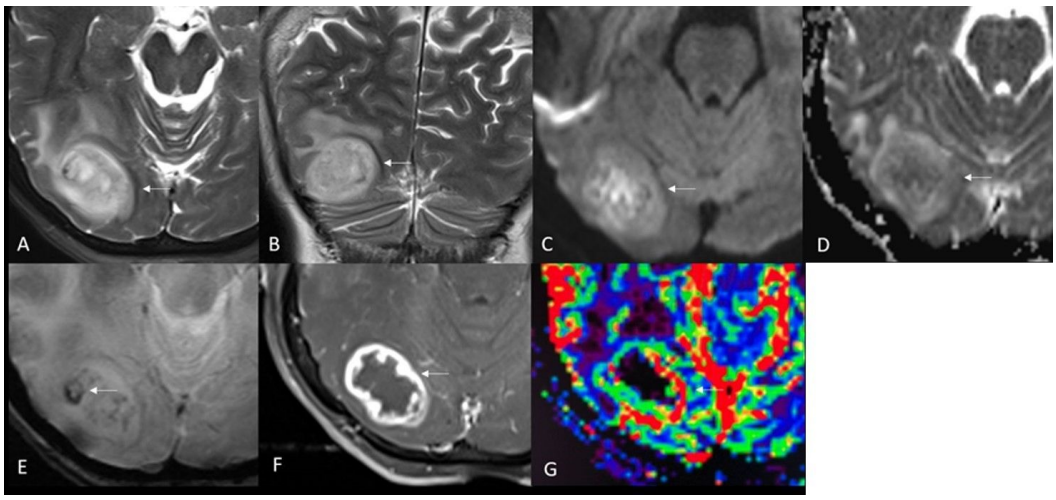

Fig. 8. A 60-year-old female patient with glioblastoma complaining of headache, visual deficiency and nausea lasting for 4 days underwent MRI for evaluation of a mass. (A,B) The axial and coronal plane T2-weighted images show a lesion located at the right occipital lobe, accompanied by oedema (arrows). The periphery of the lesion is T2 hypointense (arrow). (C,D) DWI and ADC maps of the lesion show diffusion restriction at the central portion of the lesion (arrows). (E) Intratumoural susceptibility is observed in the lesion on the SWI image (arrow). (F) The post-contrast image lesion shows ring enhancement (arrow). The peripheric part of the lesion is hyperperfused on the perfusion image (G). Using the equation mentioned in the text, we found $(1 \times 2) - (60 \times 0.05) + (1 \times 2) + 0 + (1 \times 2) - 4 = -24$. The negative result of the equation suggests a tumoral lesion.

British Journal of Hospital Medicine | 2024 | https://doi.org/10.12968/hmed.2024.0195

Imaging Findings

Both GBMs and metastases have thick, irregular wall structures (Fig. 9). While GBMs are mostly observed as heterogeneous due to bleeding and necrosis, metastases can be both solid and ring-enhanced. In immunocompromised patients, PCNSL may show ring enhancement similar to GBM (in 16.7% of cases) (Hung et al, 2023) (Fig. 10). Open ring enhancement is never seen in GBM but may be seen in 33.3% of PCNSL cases (Hung et al, 2023). Infratentorial lesions are not expected in PCNSL or GBM (Chan and Siu, 2021). Like GBM, PCNSL can cross the corpus callosum, but metastases are less likely to cross the corpus callosum than GBM (14.7% vs 5.4%) (Chan and Siu, 2021; Meier et al, 2020). While metastases tend to involve the grey-white matter junction, ependymal spread is more common in GBM than in metastases (52.9% vs 12.2%) (Meier et al, 2020). Although diffusion restriction can be observed in the central part of GBMs, it is not as homogeneous as in pyogenic abscesses (Chan and Siu, 2021). Diffusion restriction is not expected in the central part of metastases (Chan and Siu, 2021; Duygulu et al, 2010). However, diffusion restriction may be detected in lung, breast, colon and testicular tumour metastases (Duygulu et al, 2010). In GBM and metastasis, a large hyperintensity is observed around the enhancing lesion (Tepe et al, 2021). While the hyperintensity observed around metastases is entirely due to vasogenic oedema, in GBM, tumour foci spreading throughout the white matter are seen in peritumoral oedemic areas (Claes et al, 2007; Pekmezci and Perry, 2013) (Fig. 11). The outer edge of this hyperintensity is well circumscribed in 100% of GBMs and in 45.4% of metastases (Meier et al, 2020). While MRS reveals no change in the choline/creatine ratio in areas of hyperintensity in metastases, an increase in the choline/creatine ratio is detected in these areas in GBM (Chan and Siu, 2021). A study that compared the ADC values obtained from areas of increased intensity close to the lesion and distant from the lesion revealed that if the ratio was above 1.105, it could distinguish GBM from metastasis with 92% sensitivity, 87% specificity and 90% accuracy (Tepe et al, 2021). No significant difference was observed between GBM and PCNSL in terms of ADC values in the area of peritumoral hyperintensity (Hung et al, 2023). A peritumoral hyperintensity/contrast-enhanced lesion ratio >2.35 could differentiate metastasis from GBM with 68% efficiency, 84% sensitivity and 45% specificity (Maurer et al, 2013). For the peritumoral area, a choline/n-acetyl aspartate (NAA) ratio >1.115 gave a sensitivity of 93.9%, a specificity of 93.3% and an accuracy of 93.7%, while a choline/creatine ratio >1.18 gave a sensitivity of 89.8%, a specificity of 93.3% and an accuracy of 91.1%, and an NAA/creatine ratio >1.155 gave a sensitivity of 67.3%, a specificity of 93.3% and an accuracy of 44% for distinguishing GBM from metastasis (Arévalo-Sáenz et al, 2022) (Fig. 12). MRS can differentiate GBM from lymphoma with 94.4% sensitivity and 65% specificity when the threshold value for the lesion choline/creatine ratio is taken as ≤ 1.287; and with 57.4% sensitivity and 90.7% specificity when the lipid/creatine ratio is taken as >4.95 (Feng et al, 2023).

GBMs are highly vascularised lesions characterised by glomeruloid capillary structures, simple vascular hyperplasia and immature neocapillaries (Abreu et al, 2024). Similarly, metastases are also highly vascular tumours because they show

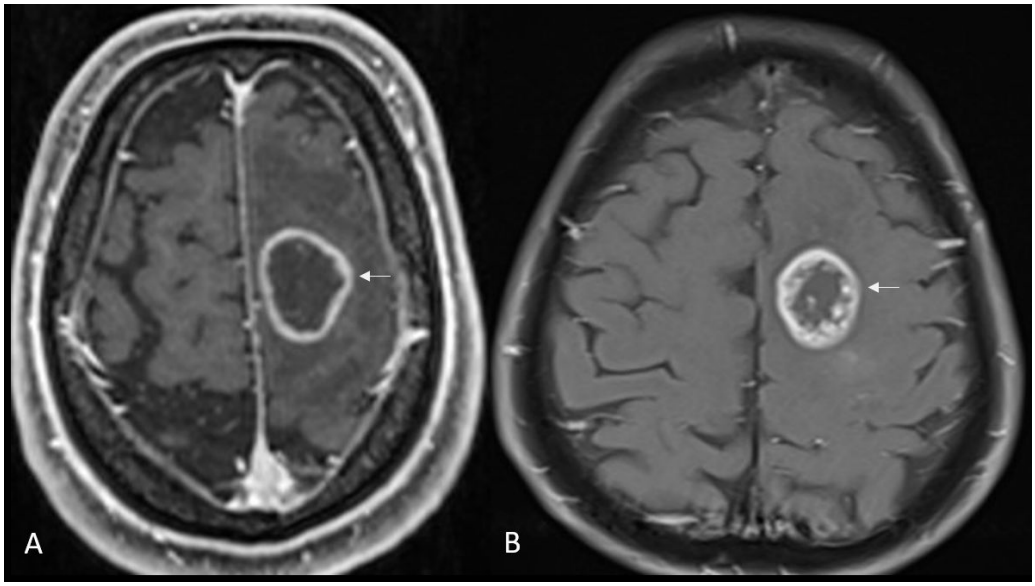

Fig. 9. (A,B) Axial post-contrast T1-weighted images of metastasis and glioblastoma. Both GBMs and metastases have thick, irregular wall structures (arrows). GBM, glioblastoma.

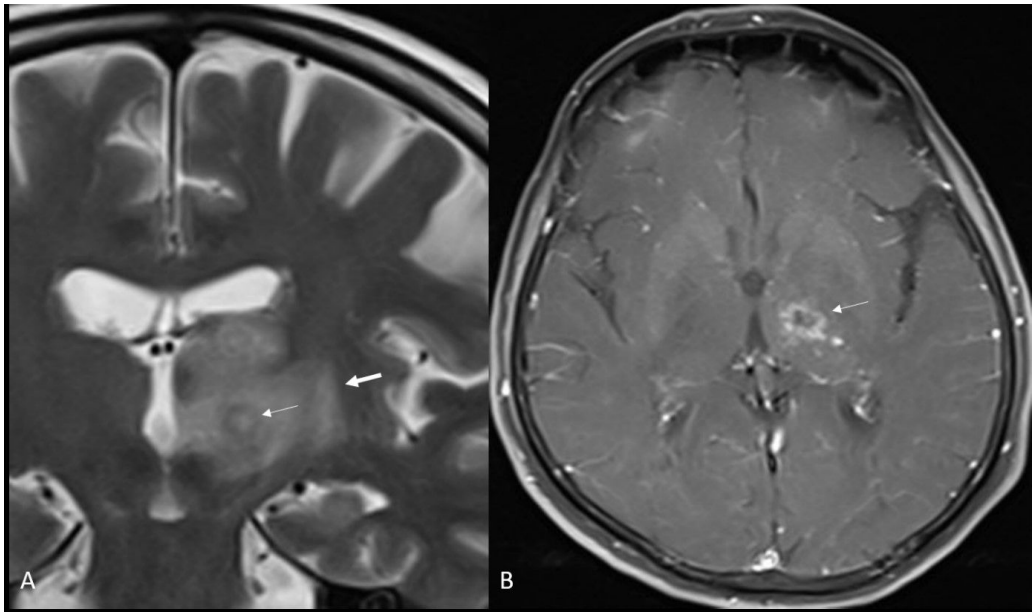

Fig. 10. A 64-year-old female presented with impaired consciousness and speech difficulty. (A) Coronal T2 weighted image shows a well circumscribed mass (a biopsy confirmed lymphoma) in the right thalamus (thin arrow) with surrounding oedema (thick arrow). The peripheral component of the lesion is T2 hypointense due to the high cellularity. (B) Axial post-contrast T1-weighted image shows peripheral enhancement of the lesion (arrow).

similar structural changes to the primary systemic lesion (Abreu et al, 2024). In PCNSL, angiocentric growth dominates and neovascularisation is not a prominent feature (Abreu et al, 2024). However, rCBV values do not discriminate between GBM and metastasis (Abreu et al, 2024) (Fig. 13), whereas rCBV values can discriminate between GBM and PCNSL (threshold value: 2.82, sensitivity: 78.6%, specificity: 92.9%, area under curve (AUC), 0.985; 95% confidence interval (CI),

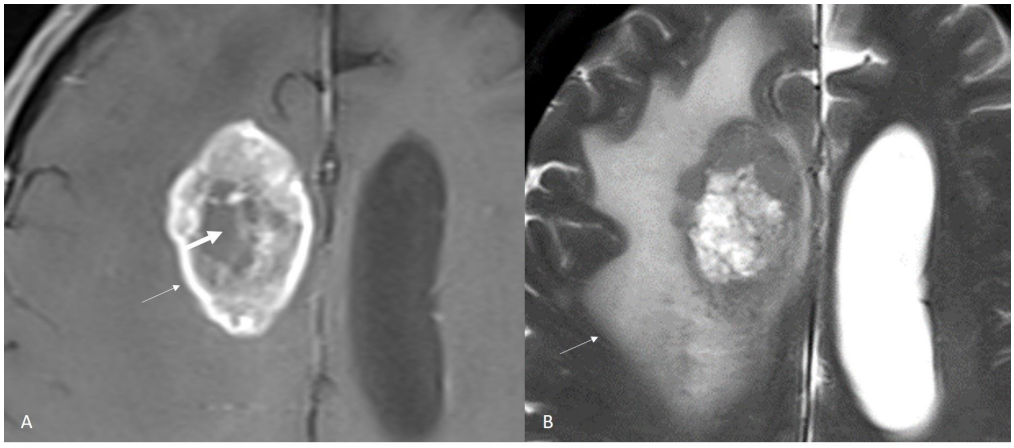

Fig. 11. A 62-year-old man with glioblastoma. (A) Axial post-contrast T1-weighted image. Ring enhancement corresponds to the highly cellular component of the GBM (thin arrow). Central necrotic component (thick arrow) is hypointense. (B) Large hyperintensity (arrow) is observed around the enhancing lesion on the axial T2-weighted image due to tumour foci spreading throughout the white matter and to oedema.

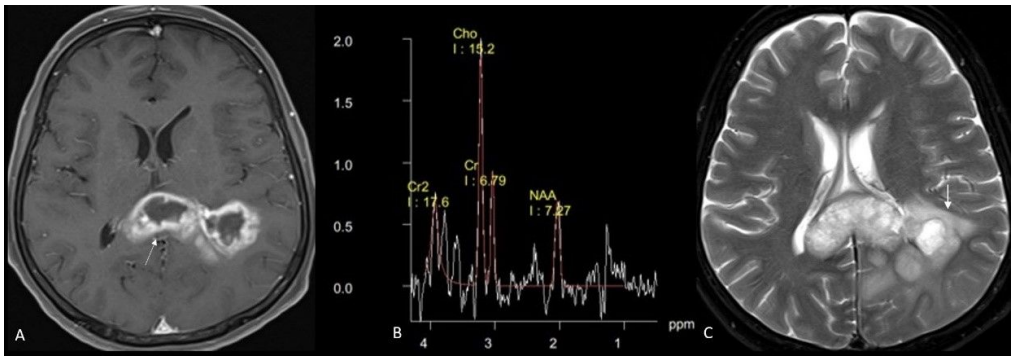

Fig. 12. A 55-year-old woman with GBM. (A) Axial post-contrast T1 weighted image shows ring-enhancing glioblastoma crossing the corpus callosum (arrow). (B,C) Magnetic resonance (MR) spectroscopy of the T2 hyperintense peritumoral area (arrow) shows a raised choline (cho) peak with a depressed n-acetyl aspartate (NAA) peak, as well as increased choline/creatine and choline/N-acetyl aspartate ratios.

0.81–0.99), as well as metastasis and PCNSL (threshold value: 2.31, sensitivity: 81.2%, specificity: 85.7%, AUC, 0.974; 95% CI, 0.74–0.99) (Abreu et al, 2024). Higher rCBV values were obtained for metastasis and GBM than for lymphoma (4.58 ± 2.54, 3.98 ± 1.87, 1.46 ± 0.29, $p < 0.001$) (Fig. 13) (Abreu et al, 2024). The percentage of signal recovery (PSR) values can also discriminate between PCNSL and metastasis (threshold value: 74.8, sensitivity 92.9%, specificity 90.9%, AUC, 0.909; 95% CI, 0.82–1.00) and PCNSL and GBM (threshold value: 82.44, sensitivity 85.7%, specificity 71.4%, AUC, 0.862; 95% CI, 0.53–0.96), as well as GBM and metastasis (threshold value: 60.35, sensitivity 85.7%, specificity 72.7%, AUC, 0.980; 95% CI, 0.53–0.96) (Abreu et al, 2024). The highest PSR value was obtained for PCNSL, followed by GBM and then metastasis (88.11; interquartile range (IQR): 21.21, 74.54; IQR: 21.23, 58.30; IQR: 22.28, respectively) (Abreu et al, 2024).

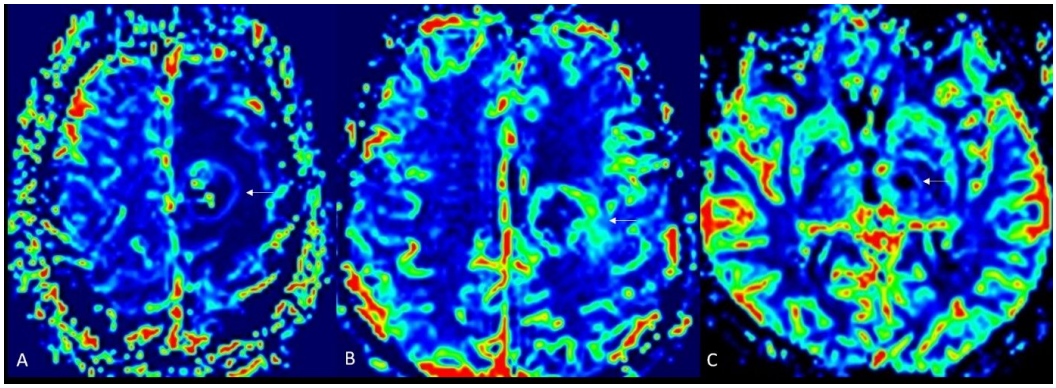

Fig. 13. (A–C) Dynamic susceptibility perfusion images of metastasis, GBM and lymphoma. Metastasis (arrow) (A) and glioblastoma (arrow) (B) both have hyperperfused areas. Higher rCBV values were obtained for metastasis and GBM than for lymphoma (arrow) (C). rCBV, relative cerebral blood volume.

A statistically significant difference was observed between PCNSL and metastasis in terms of the perfusion curve (Abreu et al, 2024). While both the descent and ascent curves are steeper in GBM, these curves are more oblique in PCNSL (Abreu et al, 2024). One report indicated that GBM and metastasis cannot be distinguished from each other using dynamic contrast-enhanced (DCE) perfusion (ktrans ($p = 0.34$) and Vp ($p = 0.47$)) (Jung et al, 2016). However, another study indicated higher mean Ve and iAUC values for PCNSL and metastasis than for high-grade gliomas ($p < 0.003$) (Zhao et al, 2015). The mean ktrans values in the peritumoral area have been reported to distinguish PCNSL from high-grade glial tumours ($p \leq 0.004$) (Zhao et al, 2015).

A ring-enhancing lesion at the sella turcica can occur with pituitary apoplexy (PA), a haemorrhagic or ischemic infarction of the gland that commonly occurs in the setting of a pituitary adenoma (Shih et al, 2021). Typical symptoms are acute-onset headache, visual deficit, ptosis, ophthalmoplaegia and vomiting (Shih et al, 2021). The appearance of PA on MRI varies depending on the stage of haemorrhage; however, PA is usually hyperintense on T1 and T2 weighted images (Shih et al, 2021; Sivaraju et al, 2017) (Fig. 14). The fluid-fluid level is highly specific for PA (Sivaraju et al, 2017). Mucosal thickening and retroclival haematoma are also suggestive of PA (Sivaraju et al, 2017).

Peripheral enhancement may be seen on post-contrast series in the rare cystic form of meningiomas (Fig. 15). Cysts may be intra- or extratumoural (Diyora et al, 2022). Differential diagnosis includes haemangioblastoma and metastases, but the extra-axial nature and broad-based attachment of the lesion to the dura is useful in differential diagnosis (Lahkim et al, 2021).

Treatment-Related Changes

GBM and metastasis are often treated by radiotherapy (Chan and Siu, 2021). Treatment-related changes may mimic residual/recurrent tumour (Chan and Siu, 2021). Radiation necrosis and pseudoprogression may occur (Brandsma et al, 2008; Chan and Siu, 2021; Sidibe et al, 2022).

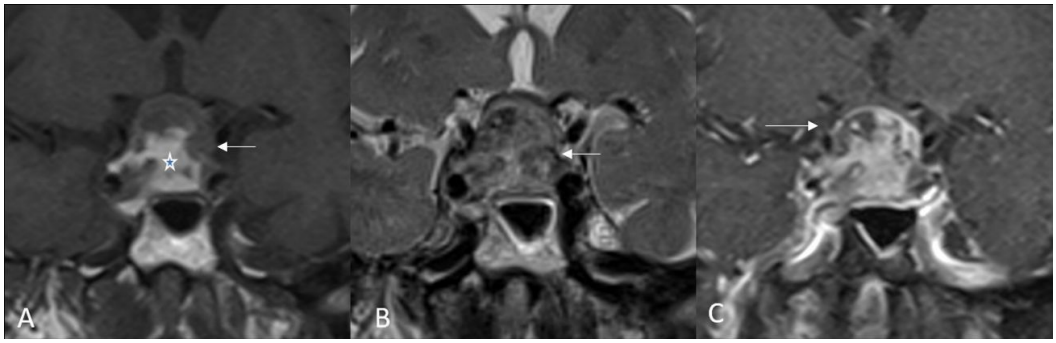

Fig. 14. A 60-year-old woman with acute onset of headache, ptosis and ophthalmoplaegia. (A) A sellar-suprasellar lesion appears hypointense on the T1 weighted MR image (arrow), with central hyperintensity corresponding to haemorrhage (star). (B) On the T2 weighted image, the lesion is hypo-hyperintense (arrow). (C) Post-contrast image reveals peripheral enhancement (arrow).

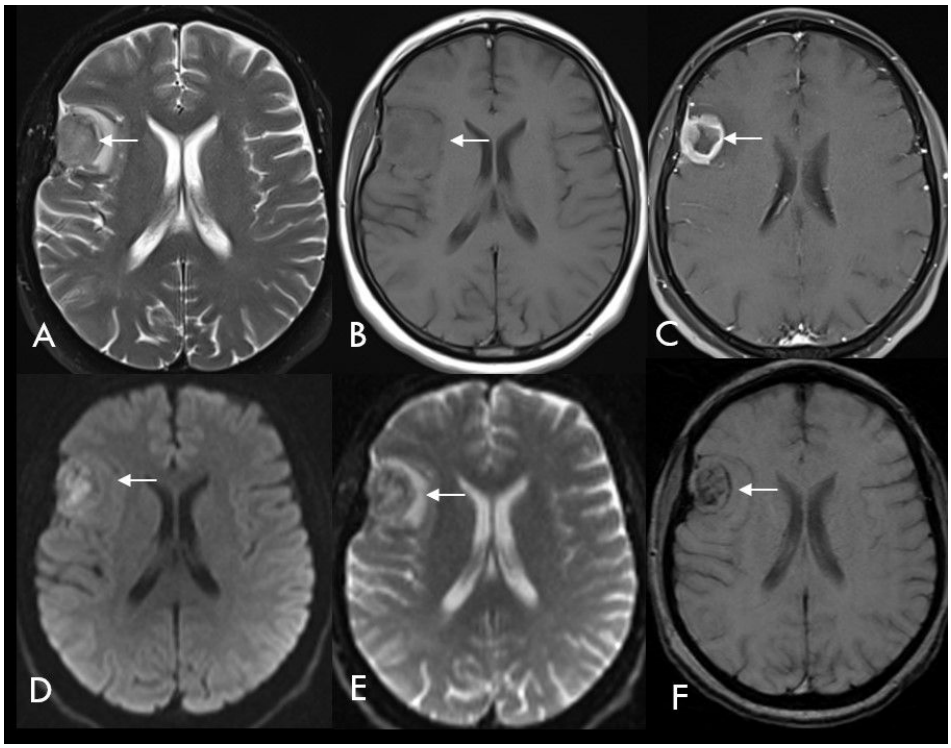

Fig. 15. Cystic meningioma in a 58-year-old female patient who presented with headache and seizures. (A,B) Axial T2 and T1 weighted images show a dural-based lesion (arrows) in the right frontal region. (C) In the post-contrast image, the periphery of the lesion is enhanced, but no contrast enhancement is visible in the centre (arrow). (D,E) Evaluation of DWI and ADC maps revealed foci showing diffusion restriction in the lesion (arrows). (F) Hypointense areas (arrow) compatible with calcification are observed in the SWI sequence.

Pseudoprogression

Pseudoprogression is a temporary increase in the number and size of contrast-enhancing lesions due to an increase in the blood-brain barrier as a result of the inflammatory response that develops within 2–6 months (median 3 months) after temozolomide and radiotherapy; it is more common in those with methylguanine-DNA methyltransferase (MGMT) methylation and is associated with tumour cell

death during chemoradiotherapy (Brandsma et al, 2008) (Fig. 15). Although contrast enhancement increases, the clinical outcomes of these patients are good and the lesions regress without additional treatment (Brandsma et al, 2008). Central diffusion restriction in a newly developed ring-enhancing lesion in a patient receiving standard chemoradiotherapy indicates pseudoprogression (Zakhari et al, 2018). This appears as an irregular ring-enhancing lesion that gradually increases in size. In perfusion MRI, the lesion appears hypoperfused due to pseudoprogression (Zhang et al, 2022) (Fig. 16). Dynamic susceptibility contrast perfusion MRI can differentiate tumour recurrence with 82% (95% CI: 0.78–0.86) accuracy and pseudoprogression with 87% (95% CI: 0.80–0.92) accuracy (Zhang et al, 2022).

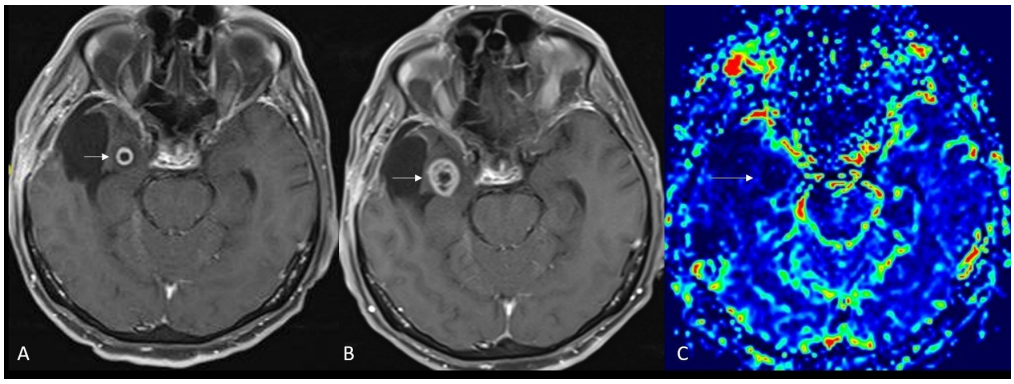

Fig. 16. A 46-year-old woman with pseudoprogression. (A) Contrast-enhanced axial T1 weighted image obtained 4 months after the operation for right temporal lobe glioblastoma treated with temozolomide and radiotherapy shows a new peripheral enhancing lesion in the right temporal lobe (arrow). (B) The size of the lesion has increased in the follow-up examination obtained 6 months after the operation (arrow). (C) Perfusion MRI shows decreased perfusion of the lesion, corresponding to pseudoprogression (arrow).

Radiation Necrosis

Radiation necrosis is the long-term effect of radiotherapy (Chan and Siu, 2021; Katsura et al, 2021; Young et al, 2011) that can be seen 6 months to years after treatment. The edges of the lesion have a ‘Swiss cheese’ or ‘soap bubble’ appearance (Katsura et al, 2021; Young et al, 2011) (Fig. 17). Corpus callosum involvement and subependymal spread are findings that are particularly suggestive of tumour recurrence (Katsura et al, 2021; Young et al, 2011). Subependymal enhancement is more common in true progression and distinguishes true from pseudoprogression with a sensitivity of 38.1%, specificity of 93.3%, and a negative predictive value of 41.8% (D’Souza et al, 2014). In MRS, a decrease in metabolites and a lactate peak are detected in the lesion (Chan and Siu, 2021). The choline/creatine ratio has been suggested as the best predictor for distinguishing between true progression and changes due to treatment effects (D’Souza et al, 2014). The absence or regression of the lesion in size supports the lesion being secondary to radiation-induced changes (Chan and Siu, 2021). Unlike pseudoprogression, no mass effect is evident in radiation necrosis, but the contrast enhancement, MRS findings and perfusion MRI findings are similar (Chan and Siu, 2021). The sensitivity of the presence of diffusion restric-

tion in differentiating glioma recurrence from radiation necrosis has been reported as 71% and the specificity as 87% (van Dijken et al, 2017). In gliomas, diffusion restriction is observed in the cellular peripheral component of the lesion, while in radiation necrosis, diffusion restriction occurs, especially in the central part (Puac-Polanco et al, 2023). Central diffusion restriction discriminates between recurrent tumour and radiation necrosis with 74% sensitivity and 89% specificity (when the threshold value is selected as $\leq 1220 \times 10^{-6}$ mm^2/s), and the AUC is 85% [95% CI (Chan and Siu, 2021), 0.70–0.94] $p < 0.0001$) (Fig. 17).

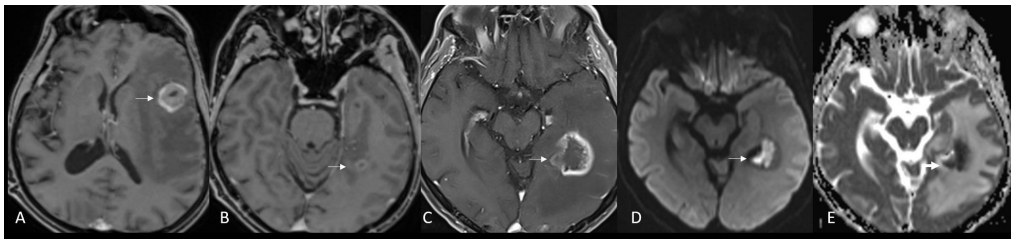

Fig. 17. A 45-year-old man with lung cancer. (A) Axial post-contrast T1 weighted image shows an enhancing metastatic lesion at the left frontal lobe (arrow). After surgery for this lesion, the patient underwent radiotherapy. (B) After 6 months, a new ring-enhancing lesion can be seen at the left temporal lobe in the field of radiotherapy (arrow). (C) The size of the lesion has increased in the follow-up examination and the edges of the lesion have a 'Swiss cheese' or 'soap bubble' appearance (arrow). (D,E) Axial DWI and ADC map show diffusion restriction in the central part of the lesion, consistent with radiation necrosis (arrows).

Haematoma

When a peripheral enhancing lesion is detected on MRI, the T1WIs should be examined, as the appearance of hematomas on post-contrast images may mimic peripheral enhancement. In the subacute phase of hematomas, the increase in extracellular methaemoglobin leads to an increase in intensity on both T1WIs and T2WIs at the periphery of the lesion and may be misleading (Chan and Siu, 2021) (Fig. 18). Chronic encapsulated intracerebral hematomas consist of a dense collagenous outer layer and an inner layer consisting of newly vascularised granulation, which causes the lesions to grow due to recurrent bleeding (Kamide et al, 2016). Hematomas are often associated with vascular malformations (Kamide et al, 2016). The capsule enhances in post-contrast series (Abou-Al-Shaar et al, 2021) and a blooming effect occurs in the gradient echo sequence at the periphery of the lesion. No increase in perfusion is observed in the lesion (Abou-Al-Shaar et al, 2021). During follow-up, the lesion size decreases (Chan and Siu, 2021).

Infarct

In ischemic situations, parenchymal enhancement occurs due to the destruction of the blood-brain barrier. Contrast enhancement begins on the third day and peaks at the end of the first week (Kanekar et al, 2012). The development of cortical laminar necrosis in the follow-up examination 2 weeks later confirms the diagnosis of infarct (Kanekar et al, 2012) (Fig. 19).

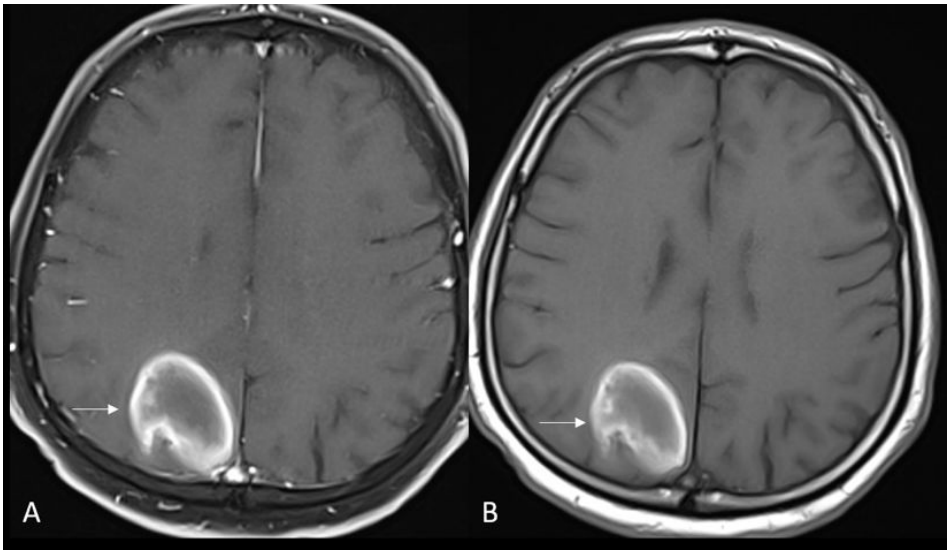

Fig. 18. Parenchymal hematoma mimicking a ring-enhancing lesion. (A) Axial post-contrast T1 weighted image shows a peripheral hyperintense lesion (arrow) at the right parietal lobe of a 60-year-old man. The appearance of hematomas on post-contrast images may mimic peripheral enhancement. When a peripheral enhancing lesion is detected on MRI, precontrast T1 weighted images should be examined. (B) The periphery of the lesion is hyperintense on precontrast T1 weighted images (arrow), consistent with subacute hematoma.

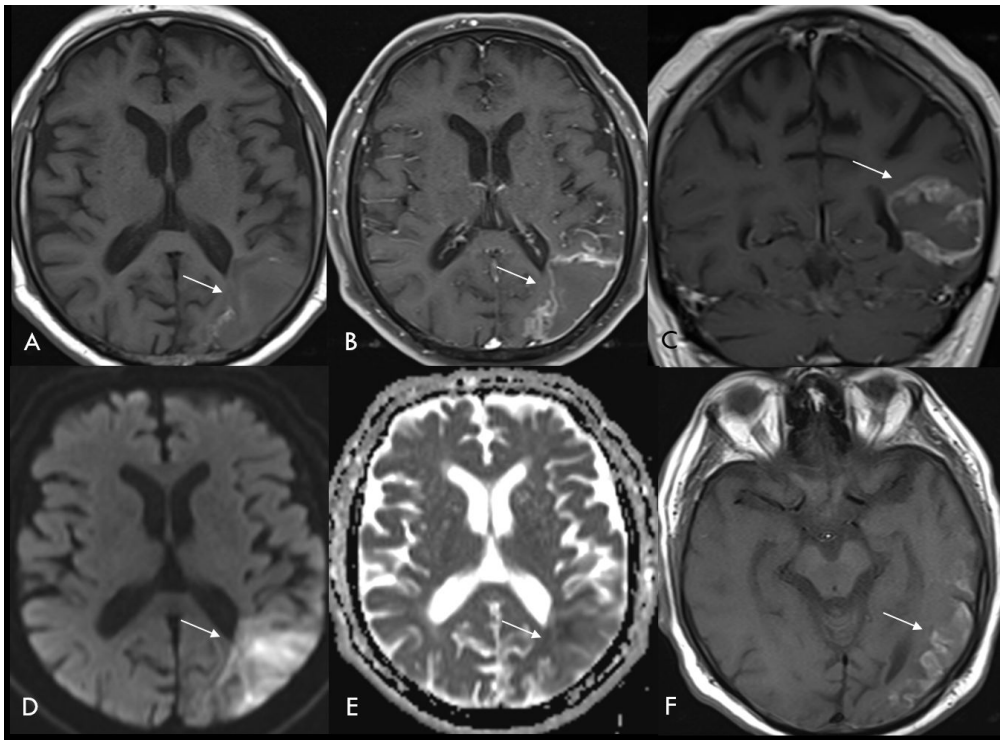

Fig. 19. Parenchymal ring enhancement due to infarction. (A) Axial T1 weighted image shows a cortical-subcortical hypo-hyperintense lesion (arrow). (B,C) Axial T1 and coronal post-contrast images reveal that the lesion is ring-enhancing (arrows). (D,E) DWI and ADC map reveal focal diffusion restriction (arrows). (F) Axial T1 weighted image obtained two weeks later shows cortical laminar necrosis (arrow).

Discussion

A wide spectrum of ischemic lesions, tumours, infections and demyelinating pathologies lead to ring enhancement. While ischemic lesions are treated with anticoagulant agents, demyelinating lesions require treatment with steroids, whereas infections must be treated by targeting the causative agent and tumours must sometimes be treated with surgery and sometimes with chemoradiotherapy. Since all of these treatment options differ completely from each other, radiological diagnosis becomes very important because a brain biopsy is not always possible. Extensive information is available in the literature regarding the contrast enhancement patterns of the lesions, lesion intensity, localisation and perfusion MRI, DWI, SWI and MRS findings. In this review, we tried to summarise the literature on this broad spectrum of diseases, based on our experiences.

Conclusion

Cerebral ring-enhancing lesions are frequently encountered in routine daily practice. Being aware of their discriminative radiological features can narrow the differential diagnosis list. MRI is the preferred method for evaluating ring-enhancing lesions.

Key Points

- MR is the preferred modality for the characterisation of ring-enhancing lesions.
- Careful evaluation of imaging features may narrow the differential diagnosis list.
- Knowledge of the typical findings, such as contrast enhancement in the basal cisterns, which is characteristic of tuberculosis, facilitates the differential diagnosis.
- In cases that cannot be resolved with conventional MR findings, advanced imaging methods, such as perfusion MRI and MR spectroscopy, can be used for problem-solving.

Availability of Data and Materials

All the data of this study are included in this article.

Author Contributions

EP and SÜ designed the review study. SBU and NSYZ analyzed the data and prepared the figures. EP drafted the manuscript. All authors contributed to the important editorial changes in the manuscript. All authors read and approved the final manuscript. All authors have participated sufficiently in the work and agreed to be accountable for all aspects of the work.

Ethics Approval and Consent to Participate

All original studies involved in this review have been approved by the Ankara University Ethics Committee (approval number: i08-646-24). Written consent was obtained from the patients stating that their images could be used in scientific studies without sharing personal data or information that would reveal their identities.

Acknowledgement

Not applicable.

Funding

This research received no external funding.

Conflict of Interest

The authors declare no conflict of interest.

References

Abou-Al-Shaar H, Faramand A, Zhang X, Mallela AN, Branstetter BF, Wiley CA, et al. Chronic encapsulated expanding hematomas after stereotactic radiosurgery for intracranial arteriovenous malformations. Journal of Neurosurgery. 2021; 136: 492–502. https://doi.org/10.3171/2021.1.JNS203476

Abou Zeid N, Pirko I, Erickson B, Weigand SD, Thomsen KM, Scheithauer B, et al. Diffusion-weighted imaging characteristics of biopsy-proven demyelinating brain lesions. Neurology. 2012; 78: 1655–1662. https://doi.org/10.1212/WNL.0b013e3182574f66

Abreu VS, Tarrio J, Silva J, Almeida F, Pinto C, Freitas D, et al. Multiparametric analysis from dynamic susceptibility contrast-enhanced perfusion MRI to evaluate malignant brain tumors. Journal of Neuroimaging. 2024; 34: 257–266. https://doi.org/10.1111/jon.13183

Altintas A, Petek B, Isik N, Terzi M, Bolukbasi F, Tavsanli M, et al. Clinical and radiological characteristics of tumefactive demyelinating lesions: follow-up study. Multiple Sclerosis. 2012; 18: 1448–1453. https://doi.org/10.1177/1352458512438237

Arévalo-Sáenz A, Rodríguez-Boto A, Pedrosa Sánchez M. High-grade glioma and solitary metastasis: differentiation by spectroscopy and advanced magnetic resonance techniques. Egyptian Journal of Neurosurgery. 2022; 37: 34. https://doi.org/10.1186/s41984-022-00172-y

Brandsma D, Stalpers L, Taal W, Sminia P, van den Bent MJ. Clinical features, mechanisms, and management of pseudoprogression in malignant gliomas. The Lancet. Oncology. 2008; 9: 453–461. https://doi.org/10.1016/S1470-2045(08)70125-6

Chan K, Siu J. Magnetic resonance imaging features of cerebral ring-enhancing lesions with different aetiologies: a pictorial essay. Hong Kong Journal of Radiology. 2021; 24: 62.

Claes A, Idema AJ, Wesseling P. Diffuse glioma growth: a guerilla war. Acta Neuropathologica. 2007; 114: 443–458. https://doi.org/10.1007/s00401-007-0293-7

D'Souza MM, Sharma R, Jaimini A, Panwar P, Saw S, Kaur P, et al. 11C-MET PET/CT and advanced MRI in the evaluation of tumor recurrence in high-grade gliomas. Clinical Nuclear Medicine. 2014; 39: 791–798. https://doi.org/10.1097/RLU.0000000000000532

Diyora B, Kukreja S, Dhal G, Devani K, Patel M, Wankhede R. Extra-Axial Cystic Meningioma without Dural Attachment in an Adult: Case Report and Review of Literature. Asian Journal of Neurosurgery. 2022; 17: 173–177. https://doi.org/10.1055/s-0042-1751010

Duygulu G, Ovali GY, Calli C, Kitis O, Yünten N, Akalin T, et al. Intracerebral metastasis showing restricted diffusion: correlation with histopathologic findings. European Journal of Radiology. 2010; 74: 117–120.

https://doi.org/10.1016/j.ejrad.2009.03.004

Feng A, Li L, Huang T, Li S, He N, Huang L, et al. Differentiating glioblastoma from primary central nervous system lymphoma of atypical manifestation using multiparametric magnetic resonance imaging: A comparative study. Heliyon. 2023; 9: e15150. https://doi.org/10.1016/j.heliyon.2023.e15150

Fereidan-Esfahani M, Decker PA, Eckel Passow JE, Lucchinetti CF, Flanagan EP, Tobin WO. Population-based incidence and clinico-radiological characteristics of tumefactive demyelination in Olmsted County, Minnesota, United States. European Journal of Neurology. 2022; 29: 782–789. https://doi.org/10.1111/ene.15182

French HD. Tumefactive multiple sclerosis versus high-grade glioma: A diagnostic dilemma. Surgical Neurology International. 2021; 12: 199. https://doi.org/10.25259/SNI_901_2020

Hung ND, Anh NN, Minh ND, Huyen DK, Duc NM. Differentiation of glioblastoma and primary central nervous system lymphomas using multiparametric diffusion and perfusion magnetic resonance imaging. Biomedical Reports. 2023; 19: 82. https://doi.org/10.3892/br.2023.1664

Işık AD, Sönmez Ö, Erdemli PC, Kepenekli E, Ergenç Z, Yılmaz S, et al. A 4-Year-Old Child with a Giant Cerebral Hydatid Cyst: A Case Report. Iranian Journal of Parasitology. 2024; 19: 113–116. https://doi.org/10.18502/ijpa.v19i1.15218

Jung BC, Arevalo-Perez J, Lyo JK, Holodny AI, Karimi S, Young RJ, et al. Comparison of Glioblastomas and Brain Metastases using Dynamic Contrast-Enhanced Perfusion MRI. Journal of Neuroimaging. 2016; 26: 240–246. https://doi.org/10.1111/jon.12281

Kamide T, Seki S, Suzuki KI, Aoki T, Hirano KI, Takahashi M, et al. A chronic encapsulated intracerebral hematoma mimicking a brain tumor: Findings on arterial spin labeling of MRI. The Neuroradiology Journal. 2016; 29: 273–276. https://doi.org/10.1177/1971400916648334

Kanekar SG, Zacharia T, Roller R. Imaging of stroke: Part 2, Pathophysiology at the molecular and cellular levels and corresponding imaging changes. AJR. American Journal of Roentgenology. 2012; 198: 63–74. https://doi.org/10.2214/AJR.10.7312

Katsura M, Sato J, Akahane M, Furuta T, Mori H, Abe O. Recognizing Radiation-induced Changes in the Central Nervous System: Where to Look and What to Look For. Radiographics. 2021; 41: 224–248. https://doi.org/10.1148/rg.2021200064

Kim DS, Na DG, Kim KH, Kim JH, Kim E, Yun BL, et al. Distinguishing tumefactive demyelinating lesions from glioma or central nervous system lymphoma: added value of unenhanced CT compared with conventional contrast-enhanced MR imaging. Radiology. 2009; 251: 467–475. https://doi.org/10.1148/radiol.2512072071

Lahkim M, Andour H, Laamrani FZ, Nouali HE, Fenni JE. Cystic meningioma: A case report with a literature review. Radiology Case Reports. 2021; 16: 2958–2961. https://doi.org/10.1016/j.radcr.2021.07.016 Erratum in: Radiology Case Reports. 2023; 18: 1645–1646. https://doi.org/10.1016/j.radcr.2023.01.019.

Luthra G, Parihar A, Nath K, Jaiswal S, Prasad KN, Husain N, et al. Comparative evaluation of fungal, tubercular, and pyogenic brain abscesses with conventional and diffusion MR imaging and proton MR spectroscopy. AJNR. American Journal of Neuroradiology. 2007; 28: 1332–1338. https://doi.org/10.3174/ajnr.A0548

Malhotra HS, Jain KK, Agarwal A, Singh MK, Yadav SK, Husain M, et al. Characterization of tumefactive demyelinating lesions using MR imaging and in-vivo proton MR spectroscopy. Multiple Sclerosis. 2009; 15: 193–203. https://doi.org/10.1177/1352458508097922

Marcus C, Feizi P, Hogg J, Summerfield H, Castellani R, Sriwastava S, et al. Imaging in Differentiating Cerebral Toxoplasmosis and Primary CNS Lymphoma With Special Focus on FDG PET/CT. AJR. American Journal of Roentgenology. 2021; 216: 157–164. https://doi.org/10.2214/AJR.19.22629

Maurer MH, Synowitz M, Badakshi H, Lohkamp LN, Wüstefeld J, Schäfer ML, et al. Glioblastoma multiforme versus solitary supratentorial brain metastasis: differentiation based on morphology and magnetic resonance signal characteristics. RoFo: Fortschritte Auf Dem Gebiete Der Rontgenstrahlen Und Der Nuklearmedizin. 2013; 185: 235–240. https://doi.org/10.1055/s-0032-1330318

Meier R, Pahud de Mortanges A, Wiest R, Knecht U. Exploratory Analysis of Qualitative MR Imaging Features for the Differentiation of Glioblastoma and Brain Metastases. Frontiers in Oncology. 2020; 10: 581037. https://doi.org/10.3389/fonc.2020.581037

Nakayama M, Naganawa S, Ouyang M, Jones KA, Kim J, Capizzano AA, et al. A Review of Clinical and Imaging Findings in Tumefactive Demyelination. AJR. American Journal of Roentgenology. 2021; 217: 186–197. https://doi.org/10.2214/AJR.20.23226

Padayachy LC, Ozek MM. Hydatid disease of the brain and spine. Child's Nervous System. 2023; 39: 751–758. https://doi.org/10.1007/s00381-022-05770-7

Pekmezci M, Perry A. Neuropathology of brain metastases. Surgical Neurology International. 2013; 4: S245–55. https://doi.org/10.4103/2152-7806.111302

Puac-Polanco P, Zakhari N, Miller J, McComiskey D, Thornhill RE, Jansen GH, et al. Diagnostic Accuracy of Centrally Restricted Diffusion Sign in Cerebral Metastatic Disease: Differentiating Radiation Necrosis from Tumor Recurrence. Canadian Association of Radiologists Journal. 2023; 74: 100–109. https://doi.org/10.1177/08465371221115341

Sankhe S, Baheti A, Ihare A, Mathur S, Dabhade P, Sarode A. Perfusion magnetic resonance imaging characteristics of intracerebral tuberculomas and its role in differentiating tuberculomas from metastases. Acta Radiologica. 2013; 54: 307–312. https://doi.org/10.1258/ar.2012.120347

Seewann A, Enzinger C, Filippi M, Barkhof F, Rovira A, Gass A, et al. MRI characteristics of atypical idiopathic inflammatory demyelinating lesions of the brain: A review of reported findings. Journal of Neurology. 2008; 255: 1–10. https://doi.org/10.1007/s00415-007-0754-x

Shih RY, Schroeder JW, Koeller KK. Primary Tumors of the Pituitary Gland: Radiologic-Pathologic Correlation. Radiographics. 2021; 41: 2029–2046. https://doi.org/10.1148/rg.2021200203

Sidibe I, Tensaouti F, Roques M, Cohen-Jonathan-Moyal E, Laprie A. Pseudoprogression in Glioblastoma: Role of Metabolic and Functional MRI-Systematic Review. Biomedicines. 2022; 10: 285. https://doi.org/10.3390/biomedicines10020285

Sivaraju L, Hegde VS, Kiran NA, Ghosal N, Hegde AS. Pituitary apoplexy presenting as a peripheral rim enhancing parasellar mass lesion with dural enhancement along the tentorium. The Neuroradiology Journal. 2017; 30: 561–567. https://doi.org/10.1177/1971400917690765

Tepe M, Saylisoy S, Toprak U, Inan I. The Potential Role of Peritumoral Apparent Diffusion Coefficient Evaluation in Differentiating Glioblastoma and Solitary Metastatic Lesions of the Brain. Current Medical Imaging. 2021; 17: 1200–1208. https://doi.org/10.2174/1573405617666210316120314

Toh CH, Wei KC, Chang CN, Hsu PW, Wong HF, Ng SH, et al. Differentiation of pyogenic brain abscesses from necrotic glioblastomas with use of susceptibility-weighted imaging. AJNR. American Journal of Neuroradiology. 2012; 33: 1534–1538. https://doi.org/10.3174/ajnr.A2986

van Dijken BRJ, van Laar PJ, Holtman GA, van der Hoorn A. Diagnostic accuracy of magnetic resonance imaging techniques for treatment response evaluation in patients with high-grade glioma, a systematic review and meta-analysis. European Radiology. 2017; 27: 4129–4144. https://doi.org/10.1007/s00330-017-4789-9

Wallner-Blazek M, Rovira A, Fillipp M, Rocca MA, Miller DH, Schmierer K, et al. Atypical idiopathic inflammatory demyelinating lesions: prognostic implications and relation to multiple sclerosis. Journal of Neurology. 2013; 260: 2016–2022. https://doi.org/10.1007/s00415-013-6918-y

Young RJ, Gupta A, Shah AD, Graber JJ, Zhang Z, Shi W, et al. Potential utility of conventional MRI signs in diagnosing pseudoprogression in glioblastoma. Neurology. 2011; 76: 1918–1924. https://doi.org/10.1212/WNL.0b013e3201174e7

Zakhari N, Taccone MS, Torres C, Chakraborty S, Sinclair J, Woulfe J, et al. Diagnostic Accuracy of Centrally Restricted Diffusion in the Differentiation of Treatment-Related Necrosis from Tumor Recurrence in High-Grade Gliomas. AJNR. American Journal of Neuroradiology. 2018; 39: 260–264. https://doi.org/10.3174/ajnr.A5485

Zhang J, Wang Y, Wang Y, Xiao H, Chen X, Lei Y, et al. Perfusion magnetic resonance imaging in the differentiation between glioma recurrence and pseudoprogression: a systematic review, meta-analysis and meta-regression. Quantitative Imaging in Medicine and Surgery. 2022; 12: 4805–4822. https://doi.org/10.21037/qims-22-32

Zhao J, Yang ZY, Luo BN, Yang JY, Chu JP. Quantitative Evaluation of Diffusion and Dynamic Contrast-Enhanced MR in Tumor Parenchyma and Peritumoral Area for Distinction of Brain Tumors. PLoS ONE. 2015; 10: e0138573. https://doi.org/10.1371/journal.pone.0138573